Chemistry & Biology 13, 973–983, September 2006 DOI 10.1016/j.chembiol.2006.07.011

Quinocarmycin Analog DX-52-1 Inhibits Cell Migration and Targets Radixin, Disrupting Interactions of Radixin with Actin and CD44

Alem W. Kahsai,[1] Shoutian Zhu,[2] Duncan J. Wardrop,[2] William S. Lane,[3] and Gabriel Fenteany[1,*]
[1]Department of Chemistry
University of Connecticut
Storrs, Connecticut 06269
[2]Department of Chemistry
University of Illinois
Chicago, Illinois 60607
[3]Harvard Microchemistry and Proteomics Analysis Facility
Harvard University
Cambridge, Massachusetts 02138

Summary

In the course of screening for new small-molecule modulators of cell motility, we discovered that quinocarmycin (also known as quinocarcin) analog DX-52-1 is an inhibitor of epithelial cell migration. While it has been assumed that the main target of DX-52-1 is DNA, we identified and confirmed radixin as the relevant molecular target of DX-52-1 in the cell. Radixin is a member of the ezrin/radixin/moesin family of membrane-actin cytoskeleton linker proteins that also participate in signal transduction pathways. DX-52-1 binds specifically and covalently to the C-terminal region of radixin, which contains the domain that interacts with actin filaments. Overexpression of radixin in cells abrogates their sensitivity to DX-52-1's antimigratory activity. Small interfering RNA-mediated silencing of radixin expression reduces the rate of cell migration. Finally, we found that DX-52-1 disrupts radixin's ability to interact with both actin and the cell adhesion molecule CD44.

Introduction

Cell migration involves regulated actin cytoskeletal assembly and membrane protrusion, cell substratum adhesion for traction, actin filament disassembly behind the cell's leading edge, cell body translocation, and finally detachment from the substratum and retraction of the trailing edge of the cell (for reviews, see [1–14]). Changes in the state of the actin cytoskeleton and its coupling to the membrane and extracellular matrix are controlled by a large number of proteins, from effectors of signal transduction to actin binding proteins that determine the structure and function of the cytoskeleton. In an effort to better understand the molecular basis of cell motility, we have been screening small organic molecules for agents that affect cell migration.

We have adapted a rapid scratch-wounding assay for high-throughput screening to a cell culture system utilizing Madin-Darby canine kidney (MDCK) epithelial cells [15]. We previously found that wound closure in confluent monolayers of MDCK cells depends upon the collective active migration of multiple rows of cells from the wound's edge in a pathway involving phosphoinositides and Rac [16, 17], a member of the Rho family of small GTPases and a key regulator of cytoskeletal dynamics and cell motility (for reviews, see [18–21]). Upstream signaling to Rac in this system appears to be mediated by glycogen synthase kinase 3 [22] and the small GTPase ADP ribosylation factor 6 [23]. c-Jun N-terminal kinase is also required for MDCK cell sheet migration [24], putatively lying downstream of Rac, as in other systems (for a review, see [20]). Using the wound closure assay, we have identified a number of new inhibitors of cell migration, including locostatin, whose molecular target, Raf kinase inhibitor protein, we have implicated by multiple approaches in the positive control of epithelial cell migration [15, 25]. More recently, we have discovered a number of other inhibitors of cell motility, including quinocarmycin analog DX-52-1, which we report on here. We identified DX-52-1 as a potent inhibitor of cell migration and wound closure from the National Cancer Society (NCI) Diversity Set, wherein it is designated NSC 607097.

The natural product quinocarmycin (also known as quinocarcin, DC-52-1, or KW-2152) and its semisynthetic derivative DX-52-1 are known to have antitumor activity in a number of cancer models [26–36]. These compounds are characterized by a tetrahydroisoquinoline skeleton, as are the saframycins, ecteinascidin 743, and phthalascidin (for a review, see [37]). Quinocarmycin has been shown to possess DNA-damaging activity [27, 32, 38–40], and it has been suggested that DX-52-1 may alkylate DNA [38]. We believed, however, that alternative targets were likely to explain the antimigratory activity of DX-52-1, as other DNA-alkylating agents such as mitomycin C do not inhibit wound closure in MDCK cell monolayers [17]. DX-52-1 has also been reported to inhibit the hypoxia-inducible factor 1 transcriptional activation pathway, although the direct molecular target in this pathway has not been identified [41].

We synthesized a biotinylated derivative of DX-52-1 and found that it retained a sufficient amount of the antimigratory activity of the original free, nonbiotinylated DX-52-1 to justify pursuit of the compound's molecular target in the cell. Using this biotinylated DX-52-1, we discovered specific and covalent binding to an approximately 80 kDa protein that we subsequently purified and identified as radixin, a nonenzymatic, membrane-associated, actin binding protein [42].

Radixin is a member of the ezrin/radixin/moesin (ERM) family of membrane-cytoskeleton linkers that are important for organization of the membrane-associated cortical actin cytoskeleton, cell migration, adhesion, and proliferation (for reviews, see [43–46]). ERM proteins are present in actin-rich cell surface structures such as cell adhesion sites, membrane ruffles, filopodia, uropods, microvilli, retraction fibers, and the cleavage furrow of dividing cells. In addition, ERM proteins play roles in signal transduction, such as signaling through Rho family small GTPases, by recruiting specific regulatory molecules (for reviews, see [43–46]). They may also have

*Correspondence: gabriel.fenteany@uconn.edu

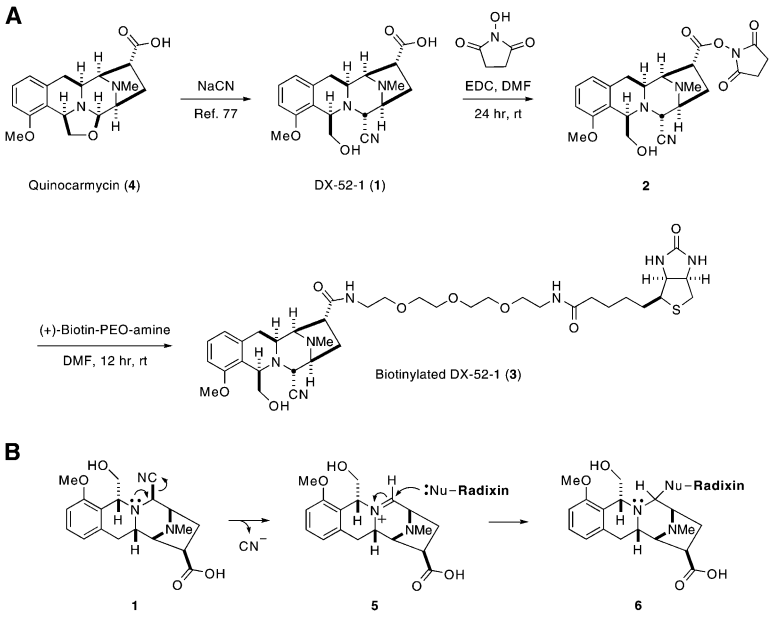

Figure 1. Synthesis of a Biotinylated Derivative of Quinocarmycin Analog DX-52-1 and Putative Mechanism of Action for Modification of Radixin by DX-52-1

(A) Quinocarmycin (also known as quinocarcin; **4**) was converted to DX-52-1 (**1**) by hydrocyanation. Biotinylated DX-52-1 (**3**) was prepared by EDC-mediated coupling of **1** to *N*-hydroxysuccinimide to yield the ester **2**, which was reacted with (+)-biotin-PEO-amine with spacer arm length of 22.9 Å to provide **3**.

(B) Putative mechanism of action for modification of radixin by DX-52-1. Decyanation of DX-52-1 (**1**) in the cell generates **5**. After initial recognition, a specific nucleophilic amino acid residue(s) (Nu) reacts with the electrophilic iminium ion of **5**, as indicated, to form the covalent complex **6**.

roles in cancer progression; the ERM-related protein merlin functions as a tumor suppressor whose mutation underlies neurofibromatosis type 2 (for a review, see [47]). DX-52-1 binds to the C-terminal region of radixin, which contains its actin binding domain. We confirmed radixin as a relevant cellular protein target of DX-52-1, first by overexpressing radixin in cells and observing a loss of the cells' sensitivity to DX-52-1's antimigratory activity, and then by RNA interference (RNAi)-based silencing of radixin expression, which resulted in delayed cell migration. Modification of radixin by DX-52-1 disrupts the interaction of radixin with actin and the cell adhesion molecule CD44, which may account for DX-52-1's ability to inhibit epithelial cell migration.

Results

Screening for Inhibitors of Wound Closure and Identification of Quinocarmycin Analog DX-52-1

We screened over 10,000 small molecules from a variety of sources, including the NCI Diversity Set, synthetic organic molecules synthesized in our lab, and those donated by colleagues. We identified seven highly potent inhibitors of cell migration with clear subtoxic antimigratory activity down to 500 nM or lower concentrations in the wound closure assay. One of these compounds, quinocarmycin analog DX-52-1 (**1** in Figure 1), has an IC_{50} value of 140 nM (Figure 2). This compound has a drug-like dose-dependent inhibitory profile and a favorable

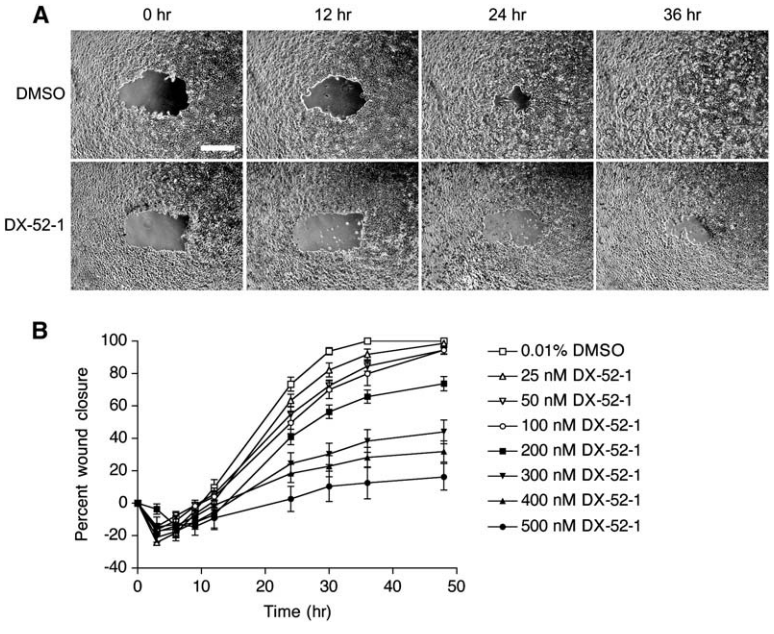

Figure 2. DX-52-1 Potently Inhibits Wound Closure in MDCK Cell Monolayers

(A) Phase contrast images taken as a function of time after treatment with 0.01% (v/v) DMSO or 300 nM DX-52-1 (treatment starting at 30 min before wounding, as in all wounding experiments). The scale bar represents 250 μm.

(B) Time course of wound closure after treatment with 0.01% DMSO (n = 15 wounded monolayers in separate wells); 25 nM DX-52-1 (n = 15); 50 nM DX-52-1 (n = 14); 100 nM DX-52-1 (n = 15); 200 nM DX-52-1 (n = 15); 300 nM DX-52-1 (n = 15); 400 nM DX-52-1 (n = 15); 500 nM DX-52-1 (n = 6). Final DMSO carrier solvent concentration was 0.01% for each treatment. The wound closure assays were conducted as previously described [15]. Data are mean ± SEM. The calculated IC_{50} value for inhibition of wound closure at 24 hr by DX-52-1 is 140 nM.

"therapeutic index" with a statistically significant minimum inhibitory concentration of 50 nM (unpaired two-tailed Student's t test for percent wound closure at 24 hr for 50 nM DX-52-1 versus 0.01% dimethyl sulfoxide [DMSO] carrier solvent control for data in Figure 2, p = 0.006) and a minimum lethal concentration of 600 nM. We ruled out that DX-52-1 inhibits cell migration by acting as a direct inhibitor of actin filament assembly. Using pyrene-labeled actin in a standard fluorescence-based in vitro assay [48, 49], we found that DX-52-1 did not affect actin polymerization (see Figure S1 in the Supplemental Data available with this article online).

DX-52-1, or 7-cyanoquinocarcinol, is the product of hydrocyanation of the natural product quinocarmycin (**4** in Figure 1). Quinocarmycin itself had only very weak subtoxic activity at 400 and 500 nM (inhibiting wound closure at 24 hr by only 22% at 500 nM, relative to parallel controls, compared to 96% inhibition for DX-52-1 at the same concentration and time point). Quinocarmycin had no activity at all at 300 nM and lower concentrations. At 600 nM and above, quinocarmycin was cytotoxic with long-term exposure. Saframycin A, which possesses the same tetrahydroisoquinoline skeleton as quinocarmycin and DX-52-1, is toxic down to 10 nM but does not appear to have any subtoxic activity below that concentration.

Synthesis of Biotinylated DX-52-1

We prepared a biotinylated derivative of DX-52-1 (**3** in Figure 1) via the synthetic route shown in Figure 1A. The structure was confirmed by nuclear magnetic resonance (NMR) and mass spectrometry (MS). This compound and the precursor ester **2** also inhibit wound closure, although not as potently as free nonbiotinylated DX-52-1, with IC_{50} values of 1.3 μM for **2** and 2.4 μM for biotinylated DX-52-1 (11% and 6% of the potency of nonbiotinylated DX-52-1, respectively). Nevertheless, this level of activity proved sufficient to purify DX-52-1 binding proteins (DBPs).

Isolation and Identification of DBPs

We observed four DBP bands at ~35, ~55, ~80, and ~120 kDa when live MDCK cells were first treated with biotinylated DX-52-1, the cells then lysed, and the resulting whole-cell extracts analyzed for biotinylated DX-52-1 binding activity (Figure 3A). The binding to all the DBPs was specific and saturable, as simultaneous addition of excess nonbiotinylated DX-52-1 completely competed away biotinylated DX-52-1 binding (Figure 3A, lane 7). The ~80 kDa DBP is by far the most intensely labeled, and is modified at lower concentrations of biotinylated DX-52-1 than the other DBPs. We found similar labeling patterns when we incubated whole-cell extracts from nontreated cells with biotinylated DX-52-1, although there also appeared some other nonspecific binding (data not shown); the DBPs are thus able to react with biotinylated DX-52-1 both in vivo and in vitro. Because in each case the DX-52-1 binding activity was visualized after adding sodium dodecyl sulfate (SDS) sample buffer, boiling, and SDS-polyacrylamide gel electrophoresis (PAGE), the interactions between DX-52-1 and the DBPs appear stable and covalent. Presumably, target alkylation occurs by reaction of a nucleophilic residue on each DBP with the electrophilic iminium ion **5** that forms upon loss of cyanide (CN^-) from DX-52-1 (Figure 1B). The formation of the reactive intermediate **5** has previously been proposed in the context of DNA alkylation [38].

Since the ~80 kDa DBP was the most strongly labeled by biotinylated DX-52-1, we purified the ~80 kDa DBP on the basis of its affinity for biotinylated DX-52-1. Upon microcapillary high-performance liquid chromatography-tandem mass spectrometry (LC-MS/MS) of tryptic fragments resulting from the ~80 kDa DBP, two individual proteins were identified: radixin, a membrane-cytoskeleton linker protein, and heat shock protein 70 (Hsp70), a ubiquitous molecular chaperone.

We confirmed that radixin is a major target of DX-52-1 by immunoprecipitation of whole-cell extracts prepared from biotinylated DX-52-1-treated live cells with an anti-radixin antibody and then detection of the biotinylated DX-52-1 binding activity (Figure 3B). We then obtained and used recombinant radixin and Hsp70 proteins for additional DX-52-1 binding and other in vitro experiments. We found that Hsp70 only bound DX-52-1 very slowly in a noncompetable and nonspecific manner (see Figure S2). In addition, DX-52-1 did not affect Hsp70 ATPase activity in vitro (see Figure S3). Furthermore, we found that treatment of MDCK cells with quercetin and KNK437, inhibitors of Hsp70 expression, had little or no effect on wound closure (see Figure S4).

In contrast, recombinant radixin bound biotinylated DX-52-1 rapidly and specifically (Figure 3C). Quinocarmycin, the parent natural product that only has very little antimigratory activity, competed only barely if at all with biotinylated DX-52-1 for binding to the DBPs, particularly radixin and the ~120 kDa DBP (see Figure S5). Using radixin truncates described previously [50, 51], we found that DX-52-1 binds a C-terminal domain fragment of radixin but not an N-terminal domain fragment (Figure 3C). We therefore sought to determine whether inhibition of radixin could explain the antimigratory activity of DX-52-1 and pursue the functional consequences of the specific reaction of radixin with DX-52-1.

Confirmation of Radixin as a Relevant Target of DX-52-1 in the Cell

We transfected constructs containing hemagglutinin (HA)-tagged radixin or green fluorescent protein (GFP)-tagged radixin into MDCK cells, selected for stably expressing cells and isolated individual cell lines. Observation of the cells by fluorescence microscopy indicates that the majority of cells in each population express the transgene, although there is some heterogeneity in expression (see Figure S6). We calculated from the intensity of bands on Western blots that the HA-radixin transgene was expressed at ~103% and the GFP-radixin transgene at ~95% that of endogenous radixin, for an approximate doubling of total radixin levels in the overall cell population in each case. We then tested the effect of DX-52-1 on wound closure in confluent monolayers of these cells. In support of the notion that radixin is a relevant cellular protein target of DX-52-1, both HA-radixin- and GFP-radixin-expressing cells were insensitive to DX-52-1's antimigratory activity at a concentration that normally strongly inhibits wound closure (Figure 4; compare to Figure 2). With both HA-radixin- and GFP-radixin-expressing cell lines, however, DX-52-1 still

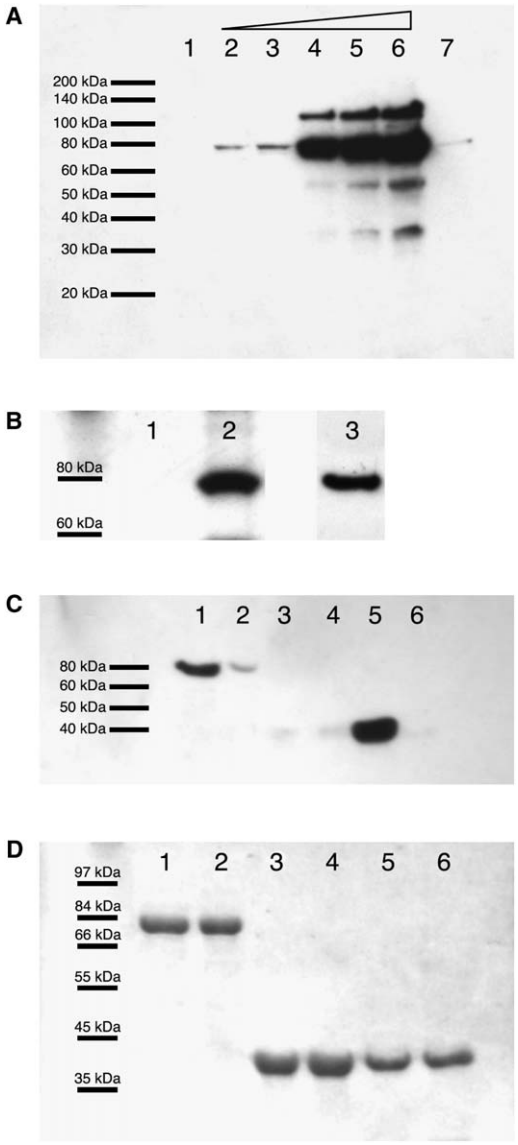

Figure 3. DX-52-1 Specifically and Covalently Binds Radixin

(A) DX-52-1 binds several proteins to varying degrees in live cells. Confluent MDCK cell cultures were incubated for 10 hr with (1) 0.05% DMSO as negative control; (2) 100 nM biotinylated DX-52-1; (3) 200 nM biotinylated DX-52-1; (4) 500 nM biotinylated DX-52-1; (5) 1 μM biotinylated DX-52-1; (6) 5 μM biotinylated DX-52-1; (7) 500 nM biotinylated DX-52-1 plus 25 μM free, nonbiotinylated DX-52-1 competitor added simultaneously. Final DMSO concentration was 0.05% for each treatment. Cells were lysed after treatment and whole-cell extracts were subjected to SDS-PAGE, followed by blotting to PVDF and chemiluminescent detection using streptavidin-HRP to visualize in vivo biotinylated proteins. Similar results were obtained when whole-cell extracts from nontreated cells were incubated with biotinylated DX-52-1. The primary DBP (~80 kDa) was purified and found to contain two proteins, radixin and Hsp70, by tandem MS. Hsp70 was subsequently ruled out as a relevant DX-52-1 target (see text).

(B) Anti-radixin antibody immunoprecipitates radixin with covalently bound biotinylated DX-52-1 from treated cells. Live MDCK cells were treated with biotinylated DX-52-1 or carrier solvent alone, lysed, and immunoprecipitated with anti-radixin antibody. After SDS-PAGE and transfer to PVDF, the blot was probed with streptavidin-HRP, followed by chemiluminescent detection. Lanes show biotinylated radixin immunoprecipitated from cells treated with (1) 0.05% DMSO as negative control; (2) 10 μM biotinylated DX-52-1. Lane 3 shows a separate Western blot of an equivalent loading as in lane 2 but probed with anti-radixin antibody.

(C) DX-52-1 binds the C-terminal region of recombinant radixin. Following incubation with biotinylated DX-52-1 in the presence or absence of excess nonbiotinylated competitor DX-52-1, recombinant protein was subjected to SDS-PAGE and Western blot analysis with streptavidin-HRP as in (A) and (B). Lanes (1) full-length radixin with 10 μM biotinylated DX-52-1; (2) full-length radixin with 10 μM biotinylated DX-52-1 plus 500 μM nonbiotinylated DX-52-1 competitor; (3) N-terminal domain fragment of radixin with 10 μM biotinylated DX-52-1; (4) N-terminal domain fragment of radixin with 10 μM biotinylated DX-52-1 plus 500 μM nonbiotinylated DX-52-1; (5) C-terminal domain fragment of radixin with 10 μM biotinylated DX-52-1; (6) C-terminal domain fragment of radixin with 10 μM biotinylated DX-52-1 plus 500 μM nonbiotinylated DX-52-1. The N-terminal domain fragment corresponds to amino acids 1–318 of murine radixin, and the C-terminal domain fragment consists of amino acids 319–583 [50, 51]. All proteins in this experiment were expressed as GST fusions, and the GST moiety was subsequently cleaved off.

(D) Coomassie blue-stained gel of equivalent sample loadings in the same order as in (C).

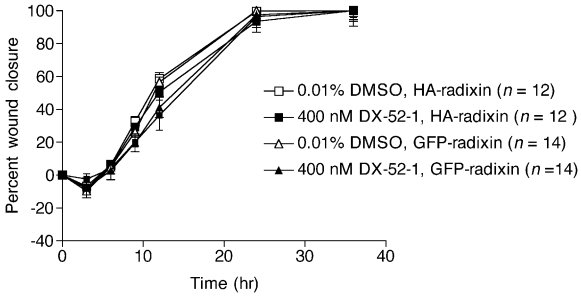

Figure 4. Overexpression of Radixin in Cells Abrogates the Inhibitory Effect of DX-52-1 on Cell Migration

Time course of wound closure in stable HA-radixin- and GFP-radixin-expressing MDCK cell monolayers after the indicated treatments. Assays were conducted as in Figure 2. Data are mean ± SEM. See Figure S6 for corresponding microscope images. Although overexpression of radixin makes the cells insensitive to the subtoxic antimigratory activity of DX-52-1, the cells are still as sensitive to the cytotoxic effects of DX-52-1 at higher concentrations with long-term exposure as normal cells, implying that toxicity is mediated by secondary targets, protein or DNA, and not radixin.

becomes cytotoxic with long-term exposure at the same higher concentrations as with normal cells.

In order to test whether loss of drug sensitivity with overexpression of radixin is specific to DX-52-1 and not just a general effect, we examined the response of radixin-overexpressing cells to locostatin, a cell migration inhibitor that is unrelated to DX-52-1 and targets Raf kinase inhibitor protein [15, 25]. We found that overexpression of radixin did not affect the sensitivity of the cells to locostatin's antimigratory activity (see Figure S7), which was similar to that of normal MDCK cells [15].

RNAi-Based Silencing of Radixin Expression

We prepared MDCK cells stably expressing a radixin-specific siRNA and control cells stably expressing an inert siRNA. The efficiency of silencing of radixin expression was >90% by Western blot analysis (Figure 5A). Wound closure in confluent monolayers of radixin knockdown cells progressed more slowly than with control cells, demonstrating a reduced rate of cell migration with radixin silencing (Figure 5B). We found that radixin

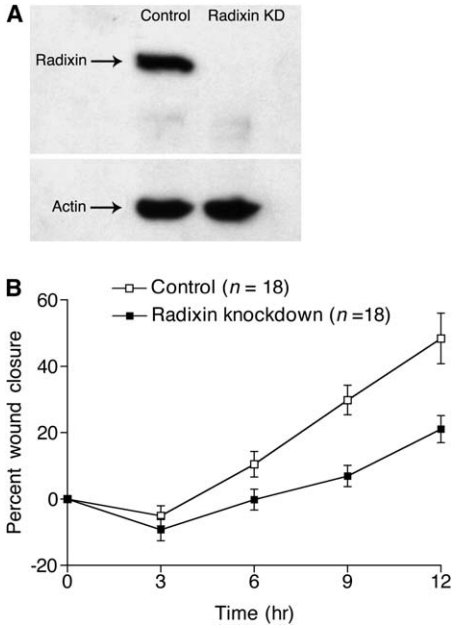

Figure 5. RNAi-Based Silencing of Radixin Expression Results in a Decreased Rate of Cell Migration

(A) Western blots of total protein from control cells stably expressing an inert siRNA and radixin knockdown MDCK cells stably expressing a radixin-specific siRNA probed with anti-radixin and anti-actin antibodies demonstrating knockdown of radixin.

(B) Time course of wound closure in confluent monolayers of control and radixin knockdown MDCK cells.

knockdown cells were rapidly killed by 400 nM DX-52-1, with lower concentrations resulting in only weak inhibition of wound closure rates below the already reduced rates of control knockdown cells (data not shown).

Effect of DX-52-1 on Interaction of Radixin with ERM Binding Proteins

It has been shown previously that ezrin adsorbed onto plastic in a solid phase binding assay exhibits filamentous actin (F-actin) binding properties characteristic of an active and not "dormant" state, and radixin binds actin similarly in this assay [52, 53]. Furthermore, ezrin binds monomeric actin (G-actin) in this system as well [52]. In other assays, although enhanced by positive regulators such as phosphoinositides, association of ERM proteins with ERM binding proteins still occurs in the absence of activation [53–55].

Using first the solid phase assay, we found that binding of radixin to F-actin is disrupted by DX-52-1 (Figure 6A). We then employed a pull-down assay and found that the interaction of radixin with F-actin in whole-cell extracts is inhibited by DX-52-1 (Figure 6B). In addition, DX-52-1 disrupts the interaction of radixin with G-actin in the solid phase assay (see Figure S8). Because of the high amounts of protein used in these assays and the following assays to facilitate detection, higher concentrations of DX-52-1 were used than in the cellular assays.

We investigated the ability of DX-52-1 to affect interactions of radixin with other known ERM binding proteins, using pull-down assays similar to those described previously [53–55]. We found that binding of radixin to CD44 is also inhibited by DX-52-1 (Figure 7). However,

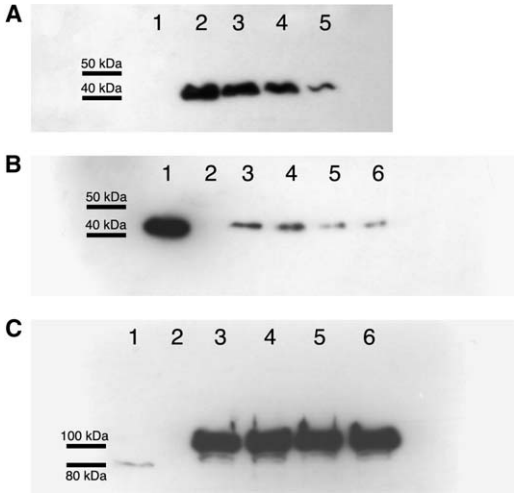

Figure 6. Interaction of Radixin with Actin Is Disrupted by DX-52-1

(A) DX-52-1 inhibits binding of radixin and F-actin in vitro in a solid phase binding assay. GST-radixin (2 μg per well adsorbed onto high protein binding capacity 96-well plates) was preincubated with DX-52-1 or carrier solvent and then allowed to bind phalloidin-stabilized F-actin added in solution (40 μg/ml actin) in F-actin buffer. Following incubation and washing, protein complexes were dissociated with SDS. The sample was then subjected to SDS-PAGE and Western blot analysis with anti-actin antibody. For a negative control, GST alone (2 μg per well) was used as above instead of GST-radixin. Lanes show actin bound to (1) GST alone; (2) GST-radixin with 1% DMSO; (3) GST-radixin with 1 μM DX-52-1; (4) GST-radixin with 5 μM DX-52-1; (5) GST-radixin with 10 μM DX-52-1. Similar results were found with baculovirally expressed nonfusion radixin protein.

(B) DX-52-1 inhibits binding of radixin and F-actin in whole-cell extracts. MDCK cell extracts in F-actin buffer containing phalloidin were subjected to pull-down with 10 μg GST-radixin (or 10 μg GST as a negative control) immobilized onto glutathione-agarose beads (and preincubated with DX-52-1 or carrier solvent prior to pull-down), followed by SDS-PAGE and Western blot analysis with anti-actin antibody. Lane 1 shows unmanipulated whole-cell extracts as a positive control. Lanes 2–6 show actin pulled down from whole-cell extracts by (2) GST alone; (3) GST-radixin with 1% DMSO; (4) GST-radixin with 1 μM DX-52-1; (5) GST-radixin with 5 μM DX-52-1; (6) GST-radixin with 10 μM DX-52-1.

(C) Loading control for lanes 1–6 in (B) showing amount of radixin present (the blot in [B] was stripped and reprobed with anti-radixin antibody).

DX-52-1 does not appear to affect the interaction of radixin with ERM binding phosphoprotein 50 (EBP50), also known as Na^+/H^+ exchanger regulatory factor (see Figure S9).

Discussion

The parent natural product, quinocarmycin, becomes cytotoxic at the same concentrations as DX-52-1, but it has little of the subtoxic antimigratory activity of DX-52-1. It is relevant to note that, unlike the cyano derivative DX-52-1 [56, 57], quinocarmycin and the related tetrazomine are capable of O_2-dependent cleavage of DNA by an alkylation-independent mechanism involving generation of superoxide ion, which dominates under aerobic conditions [56–58]. It is therefore possible that quinocarmycin is cytotoxic but has little subtoxic activity by virtue of its participation in an aerobic redox cycling pathway. Because DX-52-1 is not capable of

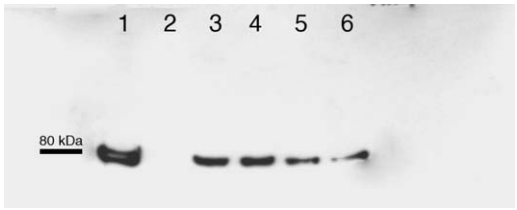

Figure 7. Interaction of Radixin with CD44 Is Disrupted by DX-52-1

One microgram of baculovirally expressed radixin, preincubated with DX-52-1 or carrier solvent, was subjected to pull-down with 10 μg GST-CD44 (or 10 μg GST alone as a negative control) immobilized onto glutathione-agarose beads, followed by SDS-PAGE and Western blot analysis with anti-radixin antibody. Lane 1 consists of radixin loaded directly as a positive control for efficacy of probing the Western blot. Lanes 2–6 show radixin pulled down by (2) GST alone; (3) GST-CD44 with 1% DMSO; (4) GST-CD44 with 1 μM DX-52-1; (5) GST-CD44 with 5 μM DX-52-1; (6) GST-CD44 with 10 μM DX-52-1.

producing superoxide or mediating oxidative scission of DNA [56, 57], it is probable that its primary mode of reactivity is the alkylation of cellular targets.

The likely mechanism of action for modification of DBPs by DX-52-1 is similar to that proposed for reaction of the quinocarmycin iminium ion **5** with DNA [38], except that, in the present case, the small molecule reacts with nucleophilic amino acid side chains rather than guanine residues of DNA (see Figure 1B). While radixin is most strongly labeled by biotinylated DX-52-1, we are also presently in the process of purifying the other secondary DBPs that show up only with higher concentrations of biotinylated DX-52-1.

Radixin, ezrin, and moesin are nonenzymatic membrane-cytoskeleton linkers whose functions have been implicated in a range of processes, particularly at actin-rich cell surface structures (for reviews, see [43–47]). To our knowledge, DX-52-1 is the first inhibitor of radixin discovered. DX-52-1 acts not by inhibiting an enzymatic activity but by disrupting protein-protein interactions. Although bioactive small molecules that inhibit protein-protein interactions are much rarer than those that target enzyme active sites (for reviews, see [59–70]), we recently discovered that another cell migration inhibitor, locostatin, which targets the signaling modulator Raf kinase inhibitor protein, also acts by disrupting protein-protein binding [25].

ERM proteins engage in a large number of protein-protein and protein-endogenous small-molecule interactions (for reviews, see [43–47]). One of their principal functions is to link the cytoskeleton to the membrane by simultaneously binding to actin filaments and membrane proteins such as CD44, a cell adhesion molecule that is a receptor for the extracellular matrix molecule hyaluronan (for reviews, see [71–74]). We found that the interaction of radixin with actin is disrupted when DX-52-1 binds radixin (Figure 6; Figure S8). Furthermore, the interaction of radixin with CD44 is also disrupted by DX-52-1 (Figure 7).

In addition to CD44, radixin is known to bind CD43 and ICAM1-3 cell adhesion molecules (for reviews, see [43–46]). ERM proteins can also interact indirectly with membrane proteins via the PDZ protein-protein interaction domain-containing proteins EBP50 and E3KARP (for reviews, see [43, 45–47]). Additional proteins from a range of functional classes are known to bind ERM proteins, including Dbl, a guanine nucleotide exchange factor that positively regulates Rho family small GTPases, and Rho guanine nucleotide dissociation inhibitor, which negatively regulates Rho proteins (for reviews, see [43–47]). Phosphoinositides bind the N-terminal 4.1/ERM (FERM) domain of ERM proteins and are involved in their activation (for reviews, see [43–47]). ERM proteins are also positively regulated by phosphorylation of their C-terminal regions by kinases such as Rho kinase, which is activated by Rho, and different isoforms of protein kinase C (for reviews, see [43, 45–47]). While we have not yet examined all of these interactions and modifications, we observed no effect of DX-52-1 on the ability of radixin to bind EBP50 (Figure S9).

DX-52-1 binds the C-terminal region of radixin (Figure 3C), while disrupting interactions of radixin with both actin filaments (Figure 6) and CD44 (Figure 7). Because the interactions with actin and CD44 occur within the C-terminal and N-terminal regions of radixin, respectively, binding of DX-52-1 appears to affect protein-protein interactions at both close range (e.g., through direct steric interference or local allosteric effects) and long range (e.g., through larger scale allosteric effects). Activation of ERM proteins enhances their association with ERM binding proteins and is thought to result from release of an autoinhibitory intramolecular interaction between the N-terminal FERM domain and the C-terminal actin binding domain (for reviews, see [43–47]). It could be hypothesized that binding of DX-52-1 promotes or favors the inactive, autoinhibited conformation of radixin, thus preventing association of the N-terminal FERM domain with CD44 and the C-terminal actin binding domain with actin. However, such a notion is not consistent with the result that the interaction of radixin with EBP50, which also involves the FERM domain, is unaffected by treatment with DX-52-1. Therefore, modification of radixin by DX-52-1 does not simply stabilize a closed, autoinhibited state of radixin. Nonetheless, it is possible that the conformational state of radixin upon binding of DX-52-1 partly mimics the inactive state, allowing certain interactions but not others. An alternative is that binding of DX-52-1 to the N-terminal domain of radixin does occur also, but the binding is either reversible or, if covalent and irreversible, only occurs with full-length protein, because of differences in organization of the N-terminal domain between full-length radixin and the fragment. We are currently exploring these possible models.

Significance

We show that quinocarmycin analog DX-52-1, whose effects on the cell were previously assumed to be mediated by alkylation of DNA, also targets the membrane-actin cytoskeleton linker and signaling protein radixin. Modification of radixin by DX-52-1 appears to explain at least part of the inhibitory effect of DX-52-1 on cell migration, as confirmed by both overexpression and siRNA-mediated silencing experiments. DX-52-1 thus represents, to our knowledge, the first known inhibitor of radixin, and it acts by disrupting the interaction of radixin with both actin and the cell adhesion protein CD44.

Experimental Procedures

Wound Closure Assay

MDCK cells were obtained from the American Type Culture Collection and cultured in growth medium (minimum essential medium with 10% [v/v] newborn calf serum) and grown to confluence at 37°C with 5% CO_2 in a humidified tissue culture incubator. All experiments were performed using early passages of MDCK cells from frozen stock cultures stored in liquid N_2. High-throughput wound closure screens were carried out in 96-well tissue culture plates, as previously described [15]. Compounds were initially screened in triplicate at a concentration of 50 μM. "Hits" at 50 μM were then rescreened at lower concentrations. Those with subtoxic inhibitory activity down to ≤500 nM were tested again with larger sample sizes over a range of concentrations to obtain dose-response profiles and IC_{50} values.

Actin Purification, Labeling, and Polymerization

Actin was prepared from rabbit muscle acetone powder according to published procedures [75, 76], with two additional rounds of polymerization-depolymerization. SDS-PAGE revealed a single band. The purified actin was then labeled with *N*-(1-pyrene)iodoacetamide (Invitrogen/Molecular Probes), and the resulting pyrene-labeled actin was used to assess the effect of DX-52-1 on the rate and extent of actin polymerization, according to established procedures [48, 49]. Briefly, pyrene-labeled G-actin (50% labeled) was added to a final concentration of 2 μM in ME buffer (50 mM $MgCl_2$, 0.2 mM ethylene glycol-*bis*(2-aminoethyl ether)-*N*,*N*,*N*′,*N*′-tetraacetic acid [EGTA]) in the presence or absence of compound in a total volume of 100 μl. After preincubation for 1 hr at 4°C, polymerization was initiated by addition of 2.5 μl 10× KMEI buffer (50 mM KCl, 1 mM $MgCl_2$, 1 mM EGTA, 10 mM imidazole [pH 7.0]) and measured by fluorescence spectrophotometry (340 nm excitation/420 nm emission).

Preparation of Biotinylated DX-52-1 (3)

DX-52-1 (1) was prepared as previously described [77]. For synthesis of 3, the biotinylated derivative of 1, a mixture of 1 (42.5 mg, 0.119 mmol, 1.0 eq), 1-ethyl-3-(3-dimethylaminopropyl)-carbodiimide hydrochloride (EDC, 34.1 mg, 0.178 mmol, 1.5 eq), and *N*-hydroxysuccinimide (34.1 mg, 0.298 mmol, 2.5 eq) in *N*,*N*-dimethylformamide (2.0 ml) was stirred at room temperature, under an N_2 atmosphere for 24 hr. The reaction mixture was then poured into a saturated aqueous $NaHCO_3$ solution (2 ml), and the product was extracted with ethyl acetate (3 × 4 ml). The organic phase was sequentially washed with water (4 ml) and saturated aqueous NaCl (4 ml), dried over Na_2SO_4, and then concentrated under reduced pressure. The remaining residue was purified by flash chromatography (silica gel, eluent: 7:3 dichloromethane/ethyl acetate) to provide the ester 2 (38.1 mg) as a yellow oil. The identity of 2 was confirmed by NMR and MS. 2 (28 mg, 0.062 mmol, 1.0 eq) was then dissolved in methanol (1.5 ml), and (+)-biotin-PEO-amine with a 22.9 Å spacer arm length (Molecular Biosciences; 52.0 mg, 0.124 mmol, 2.0 eq) was added to the solution. Progress of this reaction was monitored by thin layer chromatography. After stirring for 12 hr at room temperature the solvent was evaporated under reduced pressure, and the remaining residue was washed with ethyl acetate (2 × 3 ml) and dissolved in chloroform (1 ml). After concentration of this solution, the residue was subjected to flash chromatography (silica gel, eluent: 8.8:1.2 dichloromethane/methanol) to provide 3 (17.8 mg, 20% overall yield from 1).

Characterization of Biotinylated DX-52-1 (3)

^{1}H-NMR (400 MHz, $CDCl_3$): δ 1.23–1.58 (m, 6H), 1.50–1.80 (m, 2H), 1.99 (br s, 1H), 2.06–2.23 (m, 2H), 2.32–2.40 (m, 1H), 2.45–2.58 (m, including s at 2.50 ppm, 4H), 2.63–2.76 (m, 2H), 2.80–2.90 (m, 1H), 3.02–3.15 (m, 2H), 3.25–3.75 (m, 21H), 3.79 (s, 3H), 3.96 (br d, *J* = 2.2 Hz, 2H), 4.18–4.26 (m, 1H), 5.39 (br s, 1H), 6.06 (br s, 1H), 6.68 (d, *J* = 7.7 Hz, 1H), 6.71 (d, *J* = 8.1 Hz, 1H), 7.12 (app t, *J* = 7.9 Hz, 1H), 7.32 (br t, 1 H); ^{13}C-NMR (100.6 MHz, $CDCl_3$): 175.70, 173.26, 163.98, 155.70, 136.77, 127.55, 122.17, 120.40, 118.08, 108.29, 70.37 (2C), 69.40 (3C), 68.89, 69.73, 69.12, 64.87, 61.65, 60.14, 57.90, 57.63, 57.42, 55.37, 55.24, 44.16, 41.72, 40.55, 39.12, 39.03, 35.55, 32.73, 31.84, 27.87, 27.67, 25.41. HRMS (ESI) (*m*/*z*): [*M* + H^+] calculated for $C_{37}H_{55}N_7O_8S$, 758.3904; found, 758.3911.

Binding of Biotinylated DX-52-1 to Proteins

We initially performed experiments examining binding of biotinylated DX-52-1 to proteins in live cells. MDCK cells were plated on 100 mm diameter tissue culture plates at an initial density of 5.0 × 10^6 cells/plate in growth medium. Seven plates of confluent MDCK cell monolayers were incubated with a range of biotinylated DX-52-1 concentrations for 10 hr, with or without 50× molar excess of nonbiotinylated competitor DX-52-1 (or quinocarmycin) added simultaneously. Cells were then washed twice with phosphate-buffered saline (PBS) and lysed in ice-cold lysis buffer (20 mM Tris-HCl [pH 7.4], 150 mM NaCl, 2 mM ethylenediaminetetraacetic acid [EDTA], 2 mM dithiothreitol [DTT], 0.5% [w/v] Triton X-100, 1 μg/ml leupeptin, 1 μg/ml pepstatin A, 0.1 mM phenylmethylsulfonyl fluoride [PMSF], 0.1 mM benzamidine). After 30 min on ice, the plates were scraped with cell scrapers. Samples were homogenized by passing through a 27 gauge needle, transferred to new 1.5 ml tubes, and centrifuged (15,000 × g, 30 min, 4°C). Supernatants were concentrated to ~2 mg total protein/ml, as determined by the Bradford assay [78], in Amicon centrifugal concentrators (Millipore) with a molecular weight cutoff of 5,000 Da (4,000 × g, 4°C).

For detection of biotinylated DX-52-1 bound to proteins, equal volumes of 2× SDS sample buffer were first added to each supernatant sample, and the samples were boiled for 5 min. In addition, the pellet samples were separately resuspended in 2× SDS sample buffer. After SDS-PAGE, the proteins were electrophoretically transferred to Immobilon polyvinylidene difluoride (PVDF) membranes (Millipore). The resulting blots were blocked for 2 hr with 5% (w/v) BSA in 1% (w/v) Tween 20/Tris-buffered saline (T-TBS), then incubated with 1:1000 streptavidin-horseradish peroxidase (HRP) from Sigma in T-TBS for 1 hr. Blots were washed four times (10 min each) with T-TBS, and the biotinylated proteins were visualized using the Amersham/GE Healthcare enhanced chemiluminescence system.

We also examined binding of biotinylated DX-52-1 to proteins in whole-cell extracts in vitro. The whole-cell extracts were prepared as above in lysis buffer but from MDCK cells that had not been treated with biotinylated DX-52-1. Extracts (50 μl of a ~2 mg total protein/ml solution) were then treated with biotinylated DX-52-1, with or without addition of 50× molar excess of nonbiotinylated competitor DX-52-1 at the same time as biotinylated DX-52-1. The samples were incubated for 8 hr at 4°C on a rotating wheel. Equal volumes of 2× SDS sample buffer were then added to each sample. The samples were boiled for 5 min, then subjected to SDS-PAGE, blotted to PVDF, and probed with HRP-streptavidin as described above.

Purification of the ~80 kDa DBP

Two hundred confluent MDCK cell cultures on 100 mm diameter tissue culture plates were treated with 10 μM biotinylated DX-52-1, and whole-cell extracts were prepared as described above. All purification steps were carried out at 4°C. The "prelabeled" whole-cell extracts (~500 mg total protein) were initially fractionated by adding ammonium sulfate (AS) sequentially to 20%, 40%, 60%, and finally 80% (w/v) saturation. Each pellet was resuspended in low-salt buffer (20 mM *bis*-Tris [pH 7.0], 10 mM NaCl, 2 mM EDTA, 2 mM DTT, 1 μg/ml leupeptin, 1 μg/ml pepstatin A, 0.1 mM PMSF, 0.1 mM benzamidine). The suspensions were dialyzed overnight against the same buffer at 4°C. Samples were then centrifuged in 50 ml polycarbonate tubes (15,000 × g, 30 min, 4°C) to remove precipitates formed during dialysis.

The ~80 kDa DBP precipitated in the 60% AS pellet, while the ~120 kDa DBP came out in the 40% AS pellet, based on detection of DBPs by the procedure described earlier. The 60% AS pellet was resuspended in low-salt buffer (~120 mg total protein) and loaded onto a 5 ml HiTrap Q-sepharose anion exchange column (Amersham), preequilibrated with low-salt buffer. After washing the column with 40 ml low-salt buffer, elution was achieved with a 60 ml linear gradient of 50–400 mM NaCl. The flowthrough and all fractions were collected and resolved by SDS-PAGE, followed by detection of DBPs.

The ~80 kDa DBP eluted around 100 mM NaCl. Fractions containing the ~80 kDa DBP were combined and dialyzed overnight against low-salt buffer. To preclear nonspecific agarose binding proteins, an equal volume of agarose beads (MP Biomedical) was added as

a 1:1 slurry in low-salt buffer, and the sample was centrifuged (1,000 × g, 5 min, 4°C). The supernatant was recovered, an equal volume of streptavidin-agarose beads (Prozyme) was added as a 1:1 slurry in low-salt buffer, and the sample was incubated for 2 hr at 4°C on a rotating wheel. After centrifugation (1,000 × g, 5 min, 4°C), the beads and supernatant were separated by removing the supernatant with a micropipet. The beads were washed extensively with ice-cold PBS to remove unbound proteins, and elution of bound proteins from the beads was achieved by heating in a minimal volume of 2× SDS sample buffer. Samples were boiled for 5 min to release bound proteins, then subjected to SDS-PAGE and analyzed for DX-52-1 binding activity, with separate nonspecific protein visualization of parallel gels by silver staining. In addition, the original supernatant was also analyzed to determine the amount of protein that remained unbound.

Protein Identification

To prepare for identification of ~80 kDa DBP by LC-MS/MS, samples containing purified ~80 kDa DBP were subjected to SDS-PAGE, and the gels were stained with SYPRO Ruby dye according to the manufacturer's instructions (Invitrogen/Molecular Probes). The band corresponding to the ~80 kDa DBP was excised from the stained gels, yielding a final total of ~18 ng of the ~80 kDa DBP. Excised protein bands were subjected to in-gel reduction, *S*-carboxyamidomethylation, and digestion with trypsin. Peptide sequences were determined using a 75 μm reverse-phase microcolumn terminating in a PicoView nanoelectrospray source (New Objective) directly coupled to an LTQ linear quadrupole ion trap mass spectrometer (Thermo Electron), then analyzed as previously described [25].

Immunoprecipitation of Radixin

Live MDCK cells were treated with biotinylated DX-52-1 for 10 hr and lysed, as described earlier. The whole-cell extracts (500 μl of a ~4 mg total protein/ml solution) were precleared with 50 μl of a 1:1 slurry of protein A-sepharose beads (Invitrogen/Zymed Laboratories) in lysis buffer. Radixin was then immunoprecipitated with a goat anti-human radixin polyclonal antibody (Santa Cruz Biotechnology, sc-6408). After SDS-PAGE and transfer to PVDF, biotinylated protein was detected with streptavidin-HRP, as above.

Baculoviral Expression of Radixin

Murine radixin cDNA [79] in the pBluescript II SK(−) cloning vector was amplified by the polymerase chain reaction with 5′-ATAGC GGCCGCATGCCGAAGCCAATCAATGTAAGA-3′ and 5′-ATAGGATC CTCACATGGCTTCAAACTCATCGAT-3′ as the forward and reverse primers, respectively. The amplified product was subcloned into the NotI and BamHI sites of baculovirus transfer vector pVL1392 (BD Biosciences Pharmingen), and the primary structure of the resulting pVL1392-radixin construct was confirmed by restriction enzyme digests and DNA sequencing.

Sf9 insect cells were cultured at 27°C from cell stocks at 1–10 × 10^6 cells/ml in Sf-900 II serum-free medium (Invitrogen/GIBCO) containing 100 units/ml penicillin, 0.1 mg/ml streptomycin, and 0.25 μg/ml amphotericin B (Sigma), with rotation at 250 rpm in 500 ml spinner flasks. Recombinant virus encoding radixin was generated and amplified according to the manufacturer's instructions (BaculoGold transfection kit, BD Biosciences Pharmingen). Briefly, 60 mm diameter tissue culture plates were seeded with 2 × 10^6 cells and cotransfected with 0.5 μg linearized BaculoGold (modified AcNPV) baculovirus DNA and 4 μg pVL1392-radixin complexed with 2 ml transfection reagent. After incubation for 4 hr at 27°C, the medium was replaced. Five days after transfection, culture supernatants were collected and first-passage recombinant virus was isolated. Second-passage virus was expanded from the first-passage stock and used at a multiplicity of infection of 0.1 for generation of high-titer third-passage viral stock. Successful transfection and virus production were monitored by observing arrest of cell growth and/or cell death at later time points (4–5 days).

Purification of recombinant radixin was carried out as described previously [54], with slight modification. Sf9 cells cultured in a 2 l spinner flask were infected with recombinant virus for 72 hr at 28°C, then harvested and lysed with 30 ml of a buffer consisting of 20 mM Tris-HCl (pH 7.4), 150 mM NaCl, 2 mM EGTA, 2 mM DTT, 0.5% Triton X-100, 1 μg/ml leupeptin, 1 μg/ml pepstatin A, 0.1 mM PMSF, and 0.1 mM benzamidine. After homogenization and sonication, cell debris was removed by centrifugation (100,000 × g, 1 hr, 4°C). The supernatant was then loaded onto a 5 ml HiTrap heparin column (Amersham) which had been preequilibrated with BV buffer (10 mM HEPES [pH 7.5], 1 mM EGTA, 0.1 mM DTT). After washing the column with BV buffer, elution was achieved with a linear gradient of 150–750 mM KCl. Radixin eluted around 300 mM KCl. The eluate was dialyzed against BV buffer and then centrifuged (100,000 × g, 1 hr, 4°C). The sample was then loaded onto a preequilibrated (BV buffer) 5 ml HiTrap Q-sepharose anion exchange column (Amersham). After washing the column with BV buffer, proteins were eluted with a linear gradient of 0–200 mM KCl, and fractions were collected. The amount and purity of the recombinant radixin were analyzed by absorbance at 280 nm and SDS-PAGE. Fractions containing the highest amounts of radixin, corresponding to elution around 50 mM KCl, were pooled and dialyzed against BV buffer overnight at 4°C before flash freezing in liquid N_2 and storage at −80°C.

Expression and Purification of Other Recombinant Proteins

GST fusions of full-length and N-terminal and C-terminal domain fragments of murine radixin [51], the human cytoplasmic domain of CD44 [80] and human EBP50 [81], in the pGEX-2T, pGEX-KG, and pGEX-3X vectors, respectively, were expressed in BL21(DE3)-pLysS *Escherichia coli* cells. Single bacterial colonies were used to seed cultures in 500 ml of Luria-Bertani medium. After growing the cells overnight, isopropyl-D-thiogalactopyranoside was added to 0.2 mM, followed by incubation for 3 hr, and cells were then collected by centrifugation (5000 × g, 10 min). Bacterial pellets were resuspended in 25 ml ice-cold PBS containing 2 mM EDTA, 1 mM DTT, 1 μg/ml leupeptin, 1 μg/ml pepstatin A, 0.1 mM PMSF, and 0.1 mM benzamidine. After sonication, the lysates were diluted to 50 ml in PBS and centrifuged (15,000 × g, 30 min, 4°C). The resulting supernatants were mixed with 6 ml of a 1:1 slurry of glutathione-agarose beads (Sigma) in PBS, and then incubated on a rotating wheel for 1 hr at 4°C. Beads were washed four times with PBS, and GST-fusion proteins were eluted with 10 mM reduced glutathione (Sigma) in 50 mM Tris-HCl (pH 8.0), 150 mM NaCl, 2.5 mM $CaCl_2$, and 1 mM DTT. His_6-Hsp70 (bovine) in the pQE9 expression vector was expressed and purified on an Ni-nitrilotriacetic acid-agarose column (Qiagen), as described previously [82].

Binding of DX-52-1 to Radixin Fragments

Following expression and purification, the GST moiety was cleaved from the fusion proteins consisting of full-length radixin and N-terminal and C-terminal domain fragments of radixin by treatment with bovine thrombin (Sigma) for 24 hr at 4°C. Each recombinant protein (50 μl of 400 μg/ml solutions in a buffer of 20 mM Tris-HCl [pH 7.4], 150 mM NaCl, 2 mM EDTA, 2 mM DTT, 0.5% Triton X-100, 1 μg/ml leupeptin, 1 μg/ml pepstatin A, 100 μM PMSF, and 100 μM benzamidine) was incubated with biotinylated DX-52-1, with or without 50× excess nonbiotinylated DX-52-1 competitor added simultaneously, for 4 hr at 4°C. After adding equal volumes of 2× SDS sample buffer, samples were then subjected to SDS-PAGE, transferred to PVDF, and detected with streptavidin-HRP, as described earlier.

Hsp70 Binding and ATPase Activity

His_6-Hsp70 (50 μl of a 1.2 mg/ml solution in a buffer of 20 mM Tris-HCl [pH 7.4], 150 mM NaCl, 2 mM EDTA, 2 mM DTT, 0.5% Triton X-100, 1 μg/ml leupeptin, 1 μg/ml pepstatin A, 100 μM PMSF, and 100 μM benzamidine) was incubated with biotinylated DX-52-1, with or without 50× excess nonbiotinylated DX-52-1 competitor added simultaneously, for 4 hr at 4°C. This was followed by SDS-PAGE, transfer to PVDF, and detection with streptavidin-HRP, as above. Hsp70 ATPase activity, after preincubation of 250 μg/ml His_6-Hsp70 in the presence or absence of DX-52-1 for 4 hr at 4°C, was assayed as previously described [83–85].

Stable Transfection of MDCK Cells

To prepare stable transfectants expressing HA-radixin, MDCK cells were cotransfected at a 1:10 molar ratio with pSV2-Neo and a pMFG retroviral vector containing cDNA for murine radixin tagged at its C terminus with the HA epitope, as previously described [50]. GFP-radixin-expressing MDCK cells were prepared by transfection with

a construct encoding chicken radixin fused at its N terminus to enhanced GFP (EGFP) in the pEGFP-N1 mammalian expression vector. In both cases, transfection was mediated by lipofectamine (Invitrogen/GIBCO), following the manufacturer's instructions. Selection and maintenance of stable transfectants were carried out in growth medium with 500 μg/ml G418 sulfate (Geneticin) from Invitrogen/GIBCO. Following serial dilution of HA-radixin-expressing cells or fluorescence-activated cell sorting of GFP-radixin-expressing cells, individual cell lines were isolated from tissue culture plates containing cells at low density with sterile cloning discs for expansion on new plates. Transgene expression was evaluated by GFP fluorescence or HA immunofluorescence, as well as by Western blot analysis.

Fluorescence Observation of Cells

To visualize HA-radixin in cells, HA-radixin-expressing MDCK cells were fixed with 3.7% formaldehyde in PBS, permeabilized with 0.5% Triton X-100, and immunostained for the HA epitope with a mouse anti-HA monoclonal antibody (Santa Cruz Biotechnology, sc-7392) and an Alexa Fluor 350-conjugated goat anti-mouse IgG secondary antibody (Invitrogen/Molecular Probes, A-11068). Observation was by standard fluorescence microscopy. In many cases, cells were costained for F-actin with 50 nM tetramethylrhodamine isothiocyanate (TRITC)-labeled phalloidin (Sigma) to visualize gross actin cytoskeletal structure and actin-rich cell boundaries. GFP-radixin-expressing MDCK cells were observed both live and fixed, the latter when covisualization of F-actin with TRITC-phalloidin was desired.

siRNA-Mediated Silencing of Radixin Expression

Silencing of radixin expression was achieved using a small hairpin RNA (shRNA) expression vector modified from that previously described [22, 25]. Five potentially effective siRNA target sequences corresponding to different parts of the coding regions of canine radixin, and not found elsewhere in the canine genome (including the two other ERM proteins, ezrin and moesin), were identified with Ambion's siRNA Target Finder algorithm. The siRNA target sequences were synthesized as shRNAs and ligated into the shRNA expression vector. The constructs were then separately transfected into MDCK cells by lipofectamine-mediated transfection, according to the manufacturer's protocol (Invitrogen/GIBCO). Stable transfectants were selected in growth medium with 100 μg/ml hygromycin B (A.G. Scientific). Because the shRNA expression vector contains a GFP expression cassette [25], GFP-positive cells were isolated by fluorescence-activated cell sorter. Efficiency of knockdown was evaluated by Western blot analysis. The best knockdown was achieved with an siRNA corresponding to nucleotides 445–465 of canine radixin (GenBank accession number: XM857605). As a control for the subsequent wound closure experiments, we used a cell line expressing an siRNA corresponding to the coding region between nucleotides 1553 and 1573 of canine radixin, which we found to cause no change in radixin protein levels. Each cell line was maintained in growth medium containing 100 μg/ml hygromycin B.

Solid Phase Actin Binding

Recombinant radixin was assayed for actin binding in the presence or absence of DX-52-1 using a solid phase binding assay described previously [52]. Seventy-five microliters of GST-radixin (26.7 μg/ml), baculovirally expressed radixin (26.7 μg/ml), or GST alone as a negative control (26.7 μg/ml) was coated onto separate wells (2 μg protein per well) of Nunc MaxiSorp 96-well ELISA plates (with high protein binding capacity) in F-actin buffer (10 mM HEPES [pH 7.0], 100 mM KCl, 2 mM $MgCl_2$, 0.1 mM EGTA, 0.5 mM DTT, 0.5 mM ATP). After incubation overnight at 37°C, wells were washed with F-actin buffer. Nonspecific binding sites were blocked with 2% (w/v) bovine serum albumin. After washing wells again twice, DX-52-1 was added in 50 μl F-actin buffer. After incubation for 1 hr at room temperature, F-actin stabilized with 10 μM phalloidin (Sigma) was added to each radixin-coated well to a final concentration of 40 μg/ml actin. After another 1 hr incubation, wells were washed three times to remove unbound actin, and protein complexes were dissociated by adding 30 μl 2× SDS sample buffer to each well for 20 min at 65°C. Samples were transferred to 0.6 ml microcentrifuge tubes, boiled for 5 min, and subjected to SDS-PAGE (12% gel). Samples were blotted to PVDF for Western blot analysis with a mouse anti-actin monoclonal antibody (Sigma, A2066).

Experiments involving G-actin were done similarly to those with F-actin above, except G-actin buffer (20 mM Tris-HCl [pH 8.0], 0.2 mM $CaCl_2$, 0.5 mM DTT, 0.2 mM ATP, 0.005% NaN_3) was used instead of F-actin buffer and phalloidin was omitted in all steps. Seventy-five microliters of GST-radixin (26.7 μg/ml), baculovirally expressed radixin (26.7 μg/ml), or GST alone as a negative control (26.7 μg/ml) in G-actin buffer was coated onto separate wells (2 μg protein per well) of Nunc MaxiSorp 96-well plates, with incubation overnight at 37°C. Wells were washed with G-actin buffer, and residual binding sites were blocked with 2% BSA. Wells were washed again twice and then DX-52-1 or DMSO carrier solvent was added in 50 μl G-actin buffer. After incubation for 1 hr at room temperature, G-actin was added to a final concentration of 80 μg/ml. After another 1 hr incubation, wells were washed three times, and bound G-actin was solubilized in 30 μl 2× SDS sample buffer, followed by SDS-PAGE and Western blot analysis with anti-actin antibody.

Pull-Down of F-Actin from MDCK Cell Extracts with Recombinant Radixin

Following change of buffer to F-actin buffer, 10 μg GST-radixin or 10 μg GST alone as a negative control was immobilized onto glutathione-agarose beads (25 μl of a 1:1 slurry in F-actin buffer), and DX-52-1 or carrier solvent was added. After 30 min, whole-cell extracts (~1 mg total protein in F-actin buffer with 0.1% Tween 20 and 10 μM phalloidin) were added for a final volume of 100 μl. The beads were incubated for 2 hr at 4°C with gentle rocking, followed by three cycles of washing in the same buffer to remove unbound proteins, with centrifugation (500 × g, 1 min) between each wash to collect the beads. Bound proteins were eluted from the beads with 30 μl 2× SDS sample buffer. Following boiling, samples were subjected to SDS-PAGE and Western blot analysis with anti-actin antibody.

Pull-Down of Recombinant Radixin with GST-CD44 or GST-EBP50

These assays were done similarly to those previously described [53–55]. Ten micrograms of each GST-fusion protein or 10 μg GST alone as a negative control was immobilized onto glutathione-agarose beads (25 μl of a 1:1 slurry in PBS). Samples were then incubated with 1 μg baculovirally expressed radixin (final volume of 100 μl in PBS with 0.1% Triton X-100) that had been preincubated for 30 min with DX-52-1 or carrier solvent. After incubation for 2 hr at 4°C with gentle rocking, beads were washed three times in ice-cold PBS with 0.02% Tween 20 to remove unbound proteins. Bound proteins were eluted in 30 μl 2× SDS sample buffer, boiled, and then subjected to SDS-PAGE and Western blot analysis with anti-radixin antibody.

Supplemental Data

Supplemental Data include nine figures and are available at http://www.chembiol.com/cgi/content/full/13/9/973/DC1/.

Acknowledgments

We thank the NCI for supplying its diversity set and an additional sample of quinocarmycin analog DX-52-1 (NSC 607097), Kyowa Hakko Kogyo Company for quinocarmycin, and Andrew Myers of Harvard University for saframycin A. We thank Sachiko Tsukita of the University of Tokyo, Frank Solomon of the Massachusetts Institute of Technology, Tatyana A. Voyna-Yasenetskaya of the University of Illinois at Chicago, and Dorothy H. Crouch of the University of Dundee for radixin cDNA constructs. We also thank Rajendra K. Sharma of the University of Saskatchewan for Hsp70, Anthony Bretscher of Cornell University for EBP50, and Clare Isacke of the Institute for Cancer Research (University of London) for CD44. This work was supported by grants from the NIH (CA095177) and the American Cancer Society (RZG-02-250-01-DDC) to G.F.

Received: November 21, 2005
Revised: July 13, 2006
Accepted: July 20, 2006
Published: September 22, 2006

References

1. Small, J.V., Stradel, T., Vignal, E., and Rottner, K. (2002). The lamellipodium: where motility begins. Trends Cell Biol. *12*, 112–120.
2. Welch, M.D., and Mullins, R.D. (2002). Cellular control of actin nucleation. Annu. Rev. Cell Dev. Biol. *18*, 247–288.
3. Carlier, M.F., Clainche, C.L., Wiesner, S., and Pantaloni, D. (2003). Actin-based motility: from molecules to movement. Bioessays *25*, 336–345.
4. Fenteany, G., and Zhu, S. (2003). Small-molecule inhibitors of actin dynamics and cell motility. Curr. Top. Med. Chem. *3*, 593–616.
5. Pollard, T.D., and Borisy, G.G. (2003). Cellular motility driven by assembly and disassembly of actin filaments. Cell *112*, 453–465.
6. Ridley, A.J., Schwartz, M.A., Burridge, K., Firtel, R.A., Ginsberg, M.H., Borisy, G., Parsons, J.T., and Horwitz, A.R. (2003). Cell migration: integrating signals from front to back. Science *302*, 1704–1709.
7. Lambrechts, A., Van Troys, M., and Ampe, C. (2004). The actin cytoskeleton in normal and pathological cell motility. Int. J. Biochem. Cell Biol. *36*, 1890–1909.
8. Rafelski, S.M., and Theriot, J.A. (2004). Crawling toward a unified model of cell motility: spatial and temporal regulation of actin dynamics. Annu. Rev. Biochem. *73*, 209–239.
9. Raftopoulou, M., and Hall, A. (2004). Cell migration: Rho GTPases lead the way. Dev. Biol. *265*, 23–32.
10. Revenu, C., Athman, R., Robine, S., and Louvard, D. (2004). The co-workers of actin filaments: from cell structures to signals. Nat. Rev. Mol. Cell Biol. *5*, 635–646.
11. Disanza, A., Steffen, A., Hertzog, M., Frittoli, E., Rottner, K., and Scita, G. (2005). Actin polymerization machinery: the finish line of signaling networks, the starting point of cellular movement. Cell. Mol. Life Sci. *62*, 955–970.
12. Plastino, J., and Sykes, C. (2005). The actin slingshot. Curr. Opin. Cell Biol. *17*, 62–66.
13. Li, S., Guan, J.L., and Chien, S. (2005). Biochemistry and biomechanics of cell motility. Annu. Rev. Biomed. Eng. *7*, 105–150.
14. Webb, D.J., Zhang, H., and Horwitz, A.F. (2005). Cell migration: an overview. Methods Mol. Biol. *294*, 3–11.
15. Mc Henry, K.T., Ankala, S.V., Ghosh, A.K., and Fenteany, G. (2002). A non-antibacterial oxazolidinone derivative that inhibits epithelial cell sheet migration. ChemBioChem *3*, 1105–1111.
16. Fenteany, G., Janmey, P.A., and Stossel, T.P. (2000). Signaling pathways and cell mechanics involved in wound closure by epithelial cell sheets. Curr. Biol. *10*, 831–838.
17. Farooqui, R., and Fenteany, G. (2005). Multiple rows of cells behind an epithelial wound edge extend cryptic lamellipodia to collectively drive cell-sheet movement. J. Cell Sci. *118*, 51–63.
18. Burridge, K., and Wennerberg, K. (2004). Rho and Rac take center stage. Cell *116*, 167–179.
19. Wennerberg, K., and Der, C.J. (2004). Rho-family GTPases: it's not only Rac and Rho (and I like it). J. Cell Sci. *117*, 1301–1312.
20. Jaffe, A.B., and Hall, A. (2005). Rho GTPases: biochemistry and biology. Annu. Rev. Cell Dev. Biol. *21*, 247–269.
21. Titus, B., Schwartz, M.A., and Theodorescu, D. (2005). Rho proteins in cell migration and metastasis. Crit. Rev. Eukaryot. Gene Expr. *15*, 103–114.
22. Farooqui, R., Zhu, S., and Fenteany, G. (2006). Glycogen synthase kinase-3 acts upstream of ADP-ribosylation factor 6 and Rac1 to regulate epithelial cell migration. Exp. Cell Res. *312*, 1514–1525.
23. Santy, L.C., and Casanova, J.E. (2001). Activation of ARF6 by ARNO stimulates epithelial cell migration through downstream activation of both Rac1 and phospholipase D. J. Cell Biol. *154*, 599–610.
24. Altan, Z.M., and Fenteany, G. (2004). c-Jun N-terminal kinase regulates lamellipodial protrusion and cell sheet migration during epithelial wound closure by a gene expression-independent mechanism. Biochem. Biophys. Res. Commun. *322*, 56–67.
25. Zhu, S., Mc Henry, K.T., Lane, W.S., and Fenteany, G. (2005). A chemical inhibitor reveals the role of Raf kinase inhibitor protein in cell migration. Chem. Biol. *12*, 981–991.
26. Tomita, F., Takahashi, K., and Shimizu, K. (1983). DC-52, a novel antitumor antibiotic. 1. Taxonomy, fermentation and biological activity. J. Antibiot. (Tokyo) *36*, 463–467.
27. Tomita, F., Takahashi, K., and Tamaoki, T. (1984). Quinocarcin, a novel antitumor antibiotic. 3. Mode of action. J. Antibiot. (Tokyo) *37*, 1268–1272.
28. Chiang, C.D., Kanzawa, F., Matsushima, Y., Nakano, H., Nakagawa, K., Takahashi, H., Terada, M., Morinaga, S., Tsuchiya, R., Sasaki, Y., et al. (1987). Antitumor activity of quinocarmycin against carcinoma of the lung in human tumor clonogenic assay. J. Pharmacobiodyn. *10*, 431–435.
29. Fujimoto, K., Oka, T., and Morimoto, M. (1987). Antitumor activity of a novel antitumor antibiotic, quinocarmycin citrate (KW2152). Cancer Res. *47*, 1516–1522.
30. Inoue, S., Kubota, T., Ohishi, T., Kuzuoka, M., Oka, S., Shimoyama, Y., Kikuyama, S., Ishibiki, K., and Abe, O. (1988). Antitumor activity of quinocarmycin citrate (KW-2152) against human tumor xenografts serially transplanted into nude mice. Keio J. Med. *37*, 355–364.
31. Inaba, S., and Shimoyama, M. (1988). Antitumor activity of quinocarmycin (KW2152) against various cultured leukemia and lymphoma cell lines in vitro. Cancer Res. *48*, 6029–6032.
32. Kanamaru, R., Konishi, Y., Ishioka, C., Kakuta, H., Sato, T., Ishikawa, A., Asamura, M., and Wakui, A. (1988). The mechanism of action of quinocarmycin citrate (KW 2152) on mouse L1210 cells in vitro. Cancer Chemother. Pharmacol. *22*, 197–200.
33. Saito, H., Kobayashi, S., Uosaki, Y., Sato, A., Fujimoto, K., Miyoshi, K., Ashizawa, T., Morimoto, M., and Hirata, T. (1990). Synthesis and biological evaluation of quinocarcin derivatives. Chem. Pharm. Bull. (Tokyo) *38*, 1278–1285.
34. Saito, H., Hirata, T., Kasai, M., Fujimoto, K., Ashizawa, T., Morimoto, M., and Sato, A. (1991). Synthesis and biological evaluation of quinocarcin derivatives: thioalkyl-substituted quinones and hydroquinones. J. Med. Chem. *34*, 1959–1966.
35. Plowman, J., Dykes, D.J., Narayanan, V.L., Abbott, B.J., Saito, H., Hirata, T., and Grever, M.R. (1995). Efficacy of the quinocarmycins KW2152 and DX-52-1 against human melanoma lines growing in culture and in mice. Cancer Res. *55*, 862–867.
36. Bunnell, C.A., Supko, J.G., Eder, J.P., Jr., Clark, J.W., Lynch, T.J., Kufe, D.W., and Shulman, L.N. (2001). Phase I clinical trial of 7-cyanoquinocarcinol (DX-52-1) in adult patients with refractory solid malignancies. Cancer Chemother. Pharmacol. *48*, 347–355.
37. Scott, J.D., and Williams, R.M. (2002). Chemistry and biology of the tetrahydroisoquinoline antitumor antibiotics. Chem. Rev. *102*, 1669–1730.
38. Hill, G.C., Wunz, T.P., and Remers, W.A. (1988). Computer simulation of the binding of quinocarcin to DNA. Prediction of mode of action and absolute configuration. J. Comput. Aided Mol. Des. *2*, 91–106.
39. Flanagan, M.E., Rollins, S.B., and Williams, R.M. (1995). Netropsin and spermine conjugates of a water-soluble quinocarcin analog: analysis of sequence-specific DNA interactions. Chem. Biol. *2*, 147–156.
40. Herberich, B., Scott, J.D., and Williams, R.M. (2000). Synthesis of a netropsin conjugate of a water-soluble epi-quinocarcin analogue: the importance of stereochemistry at nitrogen. Bioorg. Med. Chem. *8*, 523–532.
41. Rapisarda, A., Uranchimeg, B., Scudiero, D.A., Selby, M., Sausville, E.A., Shoemaker, R.H., and Melillo, G. (2002). Identification of small molecule inhibitors of hypoxia-inducible factor 1 transcriptional activation pathway. Cancer Res. *62*, 4316–4324.
42. Tsukita, S., Hieda, Y., and Tsukita, S. (1989). A new 82-kD barbed end-capping protein (radixin) localized in the cell-to-cell adherens junction: purification and characterization. J. Cell Biol. *108*, 2369–2382.
43. Bretscher, A., Chambers, D., Nguyen, R., and Reczek, D. (2000). ERM-Merlin and EBP50 protein families in plasma membrane organization and function. Annu. Rev. Cell Dev. Biol. *16*, 113–143.
44. Louvet-Vallee, S. (2000). ERM proteins: from cellular architecture to cell signaling. Biol. Cell. *92*, 305–316.
45. Bretscher, A., Edwards, K., and Fehon, R.G. (2002). ERM proteins and merlin: integrators at the cell cortex. Nat. Rev. Mol. Cell Biol. *3*, 586–599.

46. Hoeflich, K.P., and Ikura, M. (2004). Radixin: cytoskeletal adopter [sic] and signaling protein. Int. J. Biochem. Cell Biol. *36*, 2131–2136.
47. McClatchey, A.I. (2003). Merlin and ERM proteins: unappreciated roles in cancer development? Nat. Rev. Cancer *3*, 877–883.
48. Kouyama, T., and Mihashi, K. (1981). Fluorimetry study of *N*-(1-pyrenyl)iodoacetamide-labelled F-actin. Local structural change of actin protomer both on polymerization and on binding of heavy meromyosin. Eur. J. Biochem. *114*, 33–38.
49. Cooper, J.A., Walker, S.B., and Pollard, T.D. (1983). Pyrene actin: documentation of the validity of a sensitive assay for actin polymerization. J. Muscle Res. Cell Motil. *4*, 253–262.
50. Henry, M.D., Gonzalez Agosti, C., and Solomon, F. (1995). Molecular dissection of radixin: distinct and interdependent functions of the amino- and carboxy-terminal domains. J. Cell Biol. *129*, 1007–1022.
51. Vaiskunaite, R., Adarichev, V., Furthmayr, H., Kozasa, T., Gudkov, A., and Voyno-Yasenetskaya, T.A. (2000). Conformational activation of radixin by G13 protein α subunit. J. Biol. Chem. *275*, 26206–26212.
52. Roy, C., Martin, M., and Mangeat, P. (1997). A dual involvement of the amino-terminal domain of ezrin in F- and G-actin binding. J. Biol. Chem. *272*, 20088–20095.
53. Barret, C., Roy, C., Montcourrier, P., Mangeat, P., and Niggli, V. (2000). Mutagenesis of the phosphatidylinositol 4,5-bisphosphate (PIP_2) binding site in the NH_2-terminal domain of ezrin correlates with its altered cellular distribution. J. Cell Biol. *151*, 1067–1080.
54. Hirao, M., Sato, N., Kondo, T., Yonemura, S., Monden, M., Sasaki, T., Takai, Y., Tsukita, S., and Tsukita, S. (1996). Regulation mechanism of ERM (ezrin/radixin/moesin) protein/plasma membrane association: possible involvement of phosphatidylinositol turnover and Rho-dependent signaling pathway. J. Cell Biol. *135*, 37–51.
55. Yonemura, S., Hirao, M., Doi, Y., Takahashi, N., Kondo, T., Tsukita, S., and Tsukita, S. (1998). Ezrin/radixin/moesin (ERM) proteins bind to a positively charged amino acid cluster in the juxta-membrane cytoplasmic domain of CD44, CD43, and ICAM-2. J. Cell Biol. *140*, 885–895.
56. Williams, R.M., Glinka, T., Flanagan, M.E., Gallegos, R., Coffman, H., and Pei, D. (1992). Cannizzaro-based O_2-dependent cleavage of DNA by quinocarcin. J. Am. Chem. Soc. *114*, 733–740.
57. Williams, R.M., Flanagan, M.E., and Tippie, T.N. (1994). O_2-dependent cleavage of DNA by tetrazomine. Biochemistry *33*, 4086–4092.
58. Williams, R.M., Glinka, T., Gallegos, R., Ehrlich, P.P., Flanagan, M.E., Coffman, H., and Park, G. (1990). Synthesis, conformation, crystal structures and DNA cleavage abilities of tetracyclic analogs of quinocarcin. Tetrahedron *47*, 2629–2642.
59. McCormick, F. (2000). Small-molecule inhibitors of cell signaling. Curr. Opin. Biotechnol. *11*, 593–597.
60. Way, J.C. (2000). Covalent modification as a strategy to block protein-protein interactions with small-molecule drugs. Curr. Opin. Chem. Biol. *4*, 40–46.
61. Cochran, A.G. (2001). Protein-protein interfaces: mimics and inhibitors. Curr. Opin. Chem. Biol. *5*, 654–659.
62. Berg, T. (2003). Modulation of protein-protein interactions with small organic molecules. Angew. Chem. Int. Ed. Engl. *42*, 2462–2481.
63. Gadek, T.R., and Nicholas, J.B. (2003). Small molecule antagonists of proteins. Biochem. Pharmacol. *65*, 1–8.
64. Sandrock, T., and Kamb, A. (2003). Non-traditional drug targets: high risk, high reward. Curr. Gene Ther. *3*, 395–404.
65. Arkin, M.R., and Wells, J.A. (2004). Small-molecule inhibitors of protein-protein interactions: progressing towards the dream. Nat. Rev. Drug Discov. *3*, 301–317.
66. Pagliaro, L., Felding, J., Audouze, K., Nielsen, S.J., Terry, R.B., Krog-Jensen, C., and Butcher, S. (2004). Emerging classes of protein-protein interaction inhibitors and new tools for their development. Curr. Opin. Chem. Biol. *8*, 442–449.
67. Arkin, M. (2005). Protein-protein interactions and cancer: small molecules going in for the kill. Curr. Opin. Chem. Biol. *9*, 317–324.
68. Fry, D.C., and Vassilev, L.T. (2005). Targeting protein-protein interactions for cancer therapy. J. Mol. Med. *12*, 955–963.
69. Yin, H., and Hamilton, A.D. (2005). Strategies for targeting protein-protein interactions with synthetic agents. Angew. Chem. Int. Ed. Engl. *44*, 4130–4163.
70. Zhao, L., and Chmielewski, J. (2005). Inhibiting protein-protein interactions using designed molecules. Curr. Opin. Struct. Biol. *15*, 31–34.
71. Isacke, C.M., and Yarwood, H. (2002). The hyaluronan receptor, CD44. Int. J. Biochem. Cell Biol. *34*, 718–721.
72. Jothy, S. (2003). CD44 and its partners in metastasis. Clin. Exp. Metastasis *20*, 195–201.
73. Ponta, H., Sherman, L., and Herrlich, P.A. (2003). CD44: from adhesion molecules to signalling regulators. Nat. Rev. Mol. Cell Biol. *4*, 33–45.
74. Marhaba, R., and Zoller, M. (2004). CD44 in cancer progression: adhesion, migration and growth regulation. J. Mol. Histol. *35*, 211–231.
75. Spudich, J.A., and Watt, S. (1971). The regulation of rabbit skeletal muscle contraction. I. Biochemical studies of the interaction of the tropomyosin-troponin complex with actin and the proteolytic fragments of myosin. J. Biol. Chem. *246*, 4866–4871.
76. Pardee, J.D., and Spudich, J.A. (1982). Purification of muscle actin. Methods Enzymol. *85*(*pt B*), 164–181.
77. Saito, H., and Tadashi, H. (1987). Synthetic approach to quinocarcin. Tetrahedron Lett. *28*, 4065–4068.
78. Bradford, M.M. (1976). A rapid and sensitive method for the quantitation of microgram quantities of protein utilizing the principle of protein-dye binding. Anal. Biochem. *72*, 248–254.
79. Funayama, N., Nagafuchi, A., Sato, N., Tsukita, S., and Tsukita, S. (1991). Radixin is a novel member of the band 4.1 family. J. Cell Biol. *115*, 1039–1048.
80. Legg, J.W., and Isacke, C.M. (1998). Identification and functional analysis of the ezrin-binding site in the hyaluronan receptor, CD44. Curr. Biol. *8*, 705–708.
81. Reczek, D., and Bretscher, A. (1998). The carboxyl-terminal region of EBP50 binds to a site in the amino-terminal domain of ezrin that is masked in the dormant molecule. J. Biol. Chem. *273*, 18452–18458.
82. Lakshmikuttyamma, A., Selvakumar, P., Anderson, D.H., Datla, R.S., and Sharma, R.K. (2004). Molecular cloning of bovine cardiac muscle heat-shock protein 70 kDa and its phosphorylation by cAMP-dependent protein kinase in vitro. Biochemistry *43*, 13340–13347.
83. Liberek, K., Marszalek, J., Ang, D., Georgopoulos, C., and Zylicz, M. (1991). *Escherichia coli* DnaJ and GrpE heat shock proteins jointly stimulate ATPase activity of DnaK. Proc. Natl. Acad. Sci. USA *88*, 2874–2878.
84. Ziegelhoffer, T., Lopez-Buesa, P., and Craig, E.A. (1995). The dissociation of ATP from hsp70 of *Saccharomyces cerevisiae* is stimulated by both Ydj1p and peptide substrates. J. Biol. Chem. *270*, 10412–10419.
85. Fewell, S.W., Smith, C.M., Lyon, M.A., Dumitrescu, T.P., Wipf, P., Day, B.W., and Brodsky, J.L. (2004). Small molecule modulators of endogenous and co-chaperone-stimulated Hsp70 ATPase activity. J. Biol. Chem. *279*, 51131–51140.